Nanoscale

ROYAL SOCIETY OF CHEMISTRY

COMMUNICATION

View Article Online
View Journal | View Issue

Cite this: *Nanoscale*, 2023, **15**, 9290

Received 6th March 2023,
Accepted 21st April 2023

DOI: 10.1039/d3nr01018j

rsc.li/nanoscale

Selection of an aggregation-caused quenching-based fluorescent tracer for imaging studies in nano drug delivery systems†

Xin Ji,[a] Yifan Cai,[c] Xiaochun Dong,[b] Wei Wu [c] and Weili Zhao [*a,b]

In order to develop and optimize nano drug delivery systems (NDDSs), it is crucial to understand their *in vivo* fate. We previously found that P2 (Aza-BODIPY) and P4 (BODIPY) as aggregation-caused quenching (ACQ) probes could be used to unravel the biofate of various nanoparticles owing to their water-sensitive emission. However, previous studies also found that quenched ACQ probe aggregates showed repartition into hydrophobic physiologically relevant constituents, resulting in fluorescence re-illumination. In this paper, we screened various types of fluorophores for ACQ and their re-illumination performance and focused on Aza-BODIPY dyes. BODIPY and Aza-BODIPY dyes were identified to be advantageous over other fluorophores. Some BODIPY and Aza-BODIPY dyes were selected as potential probes with improved performance against re-illumination. The best performing probes were Aza-C7 and Aza-C8. Aza-C7-loaded PMs were found to have decreased fluorescence re-illumination properties over P2 and DiR.

Introduction

Over the past three decades, nanotechnology has developed rapidly and been applied in drug development and clinical transformations.[1–5] Nano drug delivery systems (NDDSs), aiming at providing controlled release of drug ingredients, are a rapidly developing and remarkable nanotechnique.[6–10] In 1995, Doxil® was the first NDDS to be approved by the Food and Drug Administration (FDA) against AIDS-related Kaposi's sarcoma and ovarian cancer.[11] Though billions of dollars of investment worldwide have been applied for NDDS, only dozens of nanomedicines have been approved by the FDA up to now.[9,12,13] Hence, it has been recognized that the low clinical transition ratio is closely related to incomplete understanding of the biological fate of nanocarriers.[14]

Among various strategies available to unravel the *in vivo* fate of nanocarriers (*e.g.* CT, PET, SPECT, MRI),[6,15–19] fluorescence bioimaging of NDDSs has proved to be a valuable tool to conduct noninvasive, real-time monitoring of drug nanocarriers both in subcellular levels and *in vivo*. However, signals caused by free or dissociated fluorophores in the surroundings interfere with the results and may bias the readout of fluorescence from nanocarriers. In recent years, environmental-responsive fluorescent probes based on Förster resonance energy transfer (FRET), aggregation-induced emission (AIE), and aggregation-caused quenching (ACQ) have been developed to discriminate particle-bound signals from interfering signals in exploring the dynamics of nanocarriers.[6,19–24] FRET relies on the switching of the wavelength/intensity of the fluorescence signal following energy transfer from the donor to the acceptor depending on the environment/distance. AIE affords fluorescence enhancement upon restriction of intramolecular movement. ACQ involves fluorescence "turn off" upon aggregation at elevated concentration or declined solubility. Though ACQ was regarded to be unfavorable for fluorophores due to reduced luminance, it has recently been found to be valuable for tracking nanocarriers for drug delivery.[25,26] While FRET- and AIE-based fluorophores are well suited for

[a]*Key Laboratory for Special Functional Materials of Ministry of Education, National & Local Joint Engineering Research Center for High-efficiency Display and Lighting Technology, and School of Materials Science and Engineering, Henan University, Kaifeng, 475004, P. R. China. E-mail: zhaow@henu.edu.cn*
[b]*Department of Medicinal Chemistry, School of Pharmacy, Fudan University, Shanghai, 201203, P. R. China*
[c]*Key Laboratory of Smart Drug Delivery of MOE, School of Pharmacy, Fudan University, Shanghai 201203, P. R. China*
† Electronic supplementary information (ESI) available. See DOI: https://doi.org/10.1039/d3nr01018j

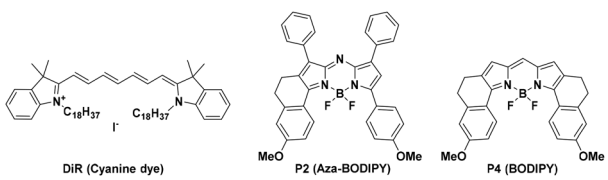

Scheme 1 Chemical structures of **DiR**, **P2** and **P4**.

in vitro studies, ACQ dyes demonstrate supremacy in exploration of the *in vivo* behaviors of drug nanocarriers over conventional fluorescent dyes, such as **DiR** (Scheme 1), as demonstrated in our previous publications.[19,27–30] **DiR** has been used for NDDS, but it usually gives confusing and misleading signals when dissociated from nanocarriers.[31–36] We accidently found that a BODIPY dye and a Aza-BODIPY dye (**P4** and **P2**, Scheme 1) selected from four dyes enable some basic requirements for bioimaging, such as high brightness, high photostability and emission at suitable wavelengths.[35] **P2** and **P4** have been successfully applied for studying the *in vivo* fate of nanocarriers.[37–48] However, repartition of quenched dye aggregates into hydrophobic physiological constituents, and the consequent re-illumination of fluorescence, may lead to pseudo-positive interference. Thus, there is a need to develop environmental-responsive ACQ fluorescent dyes with improved behavior against re-illumination while maintaining excellent ACQ properties. In this work, we screened a large library of fluorescent dyes and identified alternative Aza-BODIPY dyes with improved performance over **P2**/**P4**.

Results and discussion

ACQ properties of fluorophores with different structures

Based on the previous studies, the initial evaluation indices for absolute ACQ fluorophores mainly include the following aspects: molar extinction coefficients, wavelengths of the maximum absorption and emission, FWHM (full width at half-maximum), fluorescence quantum yields, water sensitivity and re-illumination properties in surfactant.[37–48] To validate the applicability of novel ACQ probes in nanocarriers, *in vivo* imaging experiments in polymeric micelles (PMs) need to be conducted. The primary characteristic of absolute ACQ fluorophores is good fluorescence emission in organic solvent, but with the increase of water content, its fluorescence emission rapidly decreases at a certain water content and is completely quenched in water environment. Based on the above requirements, as shown in Scheme 2, we first focused on the core structures of common fluorescent dyes and selected the following examples: 7D4MC (coumarin), Nile Red (benzoxazine dye), Cy5 DIME (cyanine dye), TMBDY (BODIPY), Rhodamine B (xanthene dye), TPP (porphyrin) and blue pigment B (phthalocyanine) for testing of the ACQ properties.

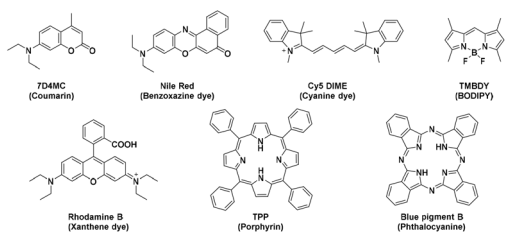

Scheme 2 Chemical structures of fluorophores with various fluorescence scaffolds.

The fluorescence spectra and intensity changes along with the content of water in acetonitrile are shown in Fig. S1 (ESI†) and Fig. 1, respectively. Among the dyes, both 7D4MC **1** and Nile Red **2** showed bathochromic shifts (433 nm to 473 nm, 615 nm to 659 nm, respectively) with the increased water content while the fluorescence intensity declined gradually. From Fig. 1a and b, it can be concluded that these dyes were not sensitive enough to the water fraction and therefore were not favorable probes. The cyanine dye with polyethene component, Cy5 DIME **3**, showed no obvious shift of the absorption band, but the response to water content was insensitive (Fig. 1b and Fig. S1c, ESI†). TMBDY **4** was more resistant to the addition of water and only showed a slight decrease of fluorescence at high water fraction (Fig. 1b and Fig. S1d, ESI†). Neither Cy5 DIME **3** nor TMBDY **4** were fully quenched on fluorescence and are suitable for use as ACQ probe for studying NDDSs. As for Rhodamine B **5** (Fig. 1c and Fig. S1e, ESI†), it was water soluble and showed strong fluorescence at around 577 nm in the aqueous environment and thus cannot act as an ACQ probe. As shown in Fig. S1f (ESI†), porphyrin dye **6** showed a complex fluorescence response to water content and exhibited emission from assembly. Although the fluorescence intensity changes at 508 nm indicated a relatively good sensitivity to water content (Fig. 1c), the complex spectrum hindered imaging application in NDDSs. As for blue pigment B **7**, the dye had poor solubility and failed to provide useful information for ACQ study. In contrast, both Aza-BODIPY (**P2**) and BODIPY (**P4**) responded nicely to water content and showed complete fluorescence quenching under a high water fraction, as shown in Fig. 1d and Fig. S1g and h (ESI†). These results were fully in agreement with our previous discovery and suggested that both Aza-BODIPY and BODIPY with sufficient

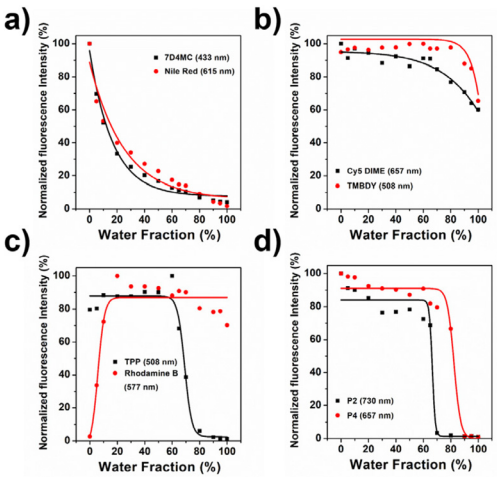

Fig. 1 Normalized fluorescence intensity (%) change of the (250 nmol L^{-1}) probes in acetonitrile/water systems. (a) For 7D4MC, excitation at 365 nm; for Nile Red, excitation at 535 nm; (b) for Cy5 DIME, excitation at 580 nm; for TMBDY, excitation at 460 nm; (c) for Rhodamine B, excitation at 510 nm; for TPP, excitation at 460 nm; (d) for P2, excitation at 680 nm; for P4, excitation at 600 nm (slit: 2/5 nm).

hydrophobicity have potential for use as fluorescence probes for NDDS.[37]

ACQ properties of various BODIPYs

The initial evaluations from the above experiments indicated that BODIPY-type fluorophores have great potential for use as ACQ probes for NDDS. To obtain further insight into the structural preferences of BODIPY, we expanded the diversity of BODIPY dyes (Scheme 3) to evaluate the ACQ properties. For rapid screening of the potential absolute ACQ fluorophores, in this part we simplified the experimental conditions. The fluorescence of each probe was tested in pure acetonitrile and pure water. Moreover, we also investigated the re-illumination, which is highly important for ACQ probes, in NDDS in both 1% Tween 80 and 1% Triton X100.[37–48]

The photophysical properties of these BODIPYs, as well as **P2**/**P4**, are presented in Table S1 (ESI†). These BODIPYs covered visible to near infrared region and showed large absorption coefficients and nice fluorescence quantum yields in acetonitrile (except **BDP-4**). The fluorescence response and fluorescence re-illumination are shown in Fig. 2. Similar to TMBDY, introduction of a 4-hydroxymethylphenyl substituent at the *meso* position (compound **BDP-1**) did not improve the ACQ property. In contrast, replacement of the two fluorine atoms on the boron with a phenylacetylene moiety significantly improved the water-responsive behavior to achieve complete fluorescence quenching in water. The re-illuminating behavior of **BDP-2** was similar to **P4** with insignificant re-illumination in 1% Tween 80 aqueous solution, but obvious re-illumination in 1% Triton X 100. Though hydrophobic modification of TMBDY resulted in ACQ, the short absorption of **BDP-2** was unfavorable. Placing a phenyl group at the 1 position of **P2** (compound **BDP-3**) led to slightly longer absorption maxima, nice ACQ and improved property against re-illumination over **P2** (Fig. 1), but the fluorescence quantum yield and absorption coefficient were lower with much declined brightness (Table S1, ESI†).

With extended conjugation, **BDP-4** maintained the nice ACQ property of hydrophobic BODIPY and exhibited similar re-illumination to **P2**. Unfortunately, even though it possessed favorable absorption maxima, the low fluorescence quantum yield and poor solubility in acetonitrile precluded its application in NDDS. We also tested a series of non-symmetric thiophene-fused BODIPYs (**BDP-5** to **BDP-10**). For the thieno[3,2-*b*]

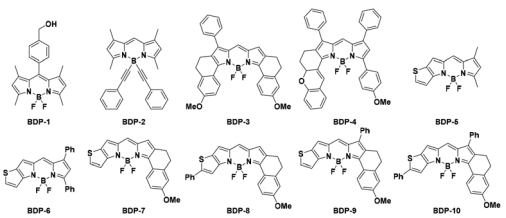

Scheme 3 Various BODIPY cores included for ACQ studies.

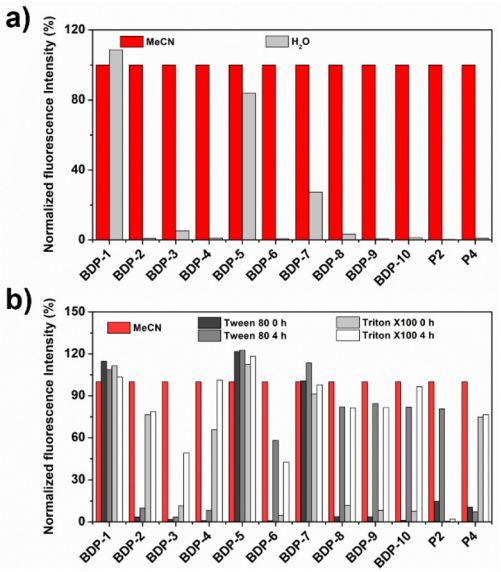

Fig. 2 (a) Normalized fluorescence intensity (%) of the probes (250 nmol L^{-1}) in acetonitrile and water. (b) Normalized fluorescence re-illumination of novel ACQ probes in surfactants 1% Tween 80 and 1% Triton X100 compared with acetonitrile. The excitation was set at the wavelength blue-shifted by 20 nm compared to the maximal absorption wavelength of each probe (slit: 5/5 nm).

pyrrole- and 2,4-dimethylpyrrole-derived BODIPY (**BDP-5**), the fluorescence was not completely quenched in water. For conformation-restricted **BDP-7**, obvious fluorescence was also noticed in water. For the 2,4-diphenylpyrrole-derived BODIPY (**BDP-6**), the ACQ property was favorable and re-illumination was minimal, but unfortunately, the short absorption maximum hindered its use for *in vivo* study of NDDS. Placing a phenyl group on the thiophene moiety (**BDP-8**), or on the conformation-restricted pyrrole (**BDP-9**), or on both (**BDP-10**), led to improved ACQ behavior and acceptable re-illumination property. Therefore, the investigations suggested that aryl-substituted BODIPY was the prerequisite structure to obtain good ACQ behavior. Interestingly, the re-illumination of **P2** in 1% Triton X 100 was insignificant, but it was more obvious in 1% Tween 80. Compared with BODIPY dyes, Aza-BODIPY **P2** possessed favorable spectroscopic properties as an NIR dye and presented excellent ACQ behavior. These results indicate that the NIR BODIPY and Aza-BODIPY dyes possess excellent ACQ behavior and were more likely to provide a solution for the re-illumination problem. Therefore, our next focus was evaluation of NIR BODIPY dyes with various substituents and rigidities. The selected examples are shown in Scheme S1 (ESI†) and the re-illumination investigations are shown in Fig. 3. The corresponding spectroscopic data are collected in Table S2 (ESI†).

All these BODIPY dyes exhibited excellent fluorescence quantum yields in acetonitrile. Thus, conformation restriction affords longer absorption maxima and larger absorption coefficients in general. For the substitution effect, it can be concluded that an electronic-rich moiety always favors the absorp-

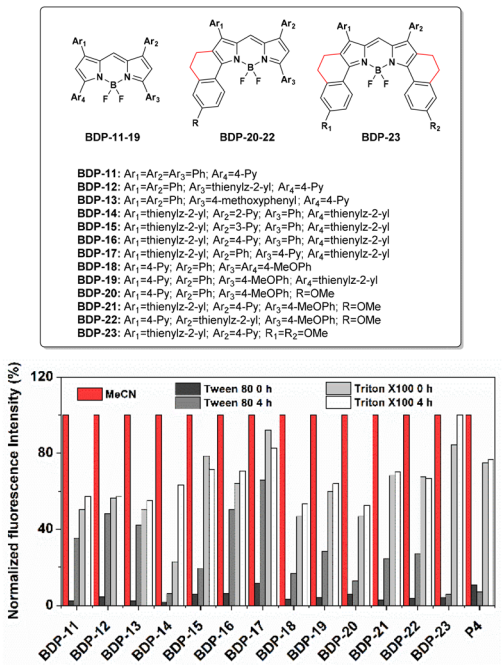

Fig. 3 Chemical structures of BODIPYs (upper panel) and normalized fluorescence re-illumination of novel ACQ probes (250 nmol L^{-1}) in surfactants 1% Tween 80 and 1% Triton X100 compared with acetonitrile (lower panel). The excitation was set at the wavelength blue-shifted by 20 nm compared to the maximal absorption wavelength of the probe (slit: 5/5 nm).

tion at longer wavelength. The fluorescence of these BODIPYs can be completely quenched in water (data not shown). In the test of fluorescence re-illumination (Fig. 3), all of the investigated BODIPY dyes emitted extremely strong fluorescence after incubation in 1% Triton X100. Overall, these BODIPYs showed similar re-illumination behavior to **P2**, but with inferior brightness. Unfortunately, structure variations on the BODIPY dyes did not seem to provide hints to overcome the re-illumination issue.

ACQ property and fluorescence re-illumination of Aza-BODIPYs

Considering the favorable NIR absorption, high fluorescence quantum yield, and excellent ACQ property of Aza-BODIPY **P2**, we then investigated a large number of Aza-BODIPYs, aiming to identify Aza-BODIPY dyes with better behavior against re-illumination. The structures of Aza-BODIPY dyes with no conformation restriction (Type A), conformation restricted on one side (Type B), and conformation restricted on two sides (Type C) with various substitutions are shown in Scheme 4 and Schemes S2–S4 (ESI†). The spectroscopic data for these Aza-BODIPYs are presented in Tables S3–S5 (ESI†). Compared with the properties of the BODIPYs, the maximum absorption and emission wavelengths of the Aza-BODIPYs were red-shifted into the NIR region with slightly diminished fluorescence quantum yields owing to the increased internal conversion. All of the Aza-BODIPY dyes revealed good to excellent ACQ behavior as desired (Fig. S3, ESI†). From the re-illumination patterns shown in Fig. 4, we were pleased to observe that many of them showed much declined re-illumination in surfactant solution compared with **P2**. Among the non-rigidified Aza-BODIPY dyes (Type A), **Aza-A4**, **Aza-A5**, **Aza-A7**, **Aza-A9**, **Aza-A13**, **Aza-A14**, **Aza-A15** were all minimally re-illuminated (Fig. 4a). These dyes all had absorption maxima longer than 680 nm and strong fluorescence (Φ_f > 0.20), and were suitable for NDDS applications. Of particular note, **Aza-A9** (732/757 nm, Φ_f of 0.22,

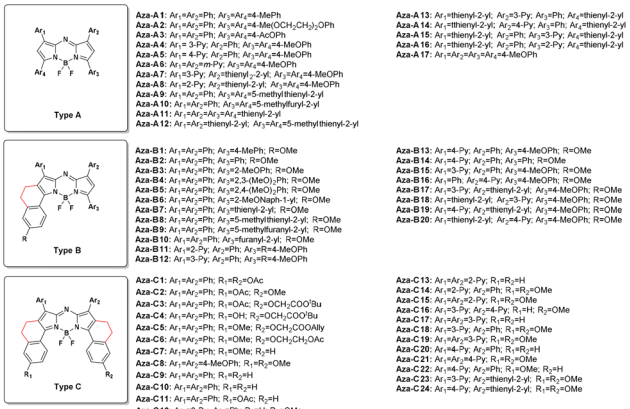

Scheme 4 Three types of tested Aza-BODIPYs.

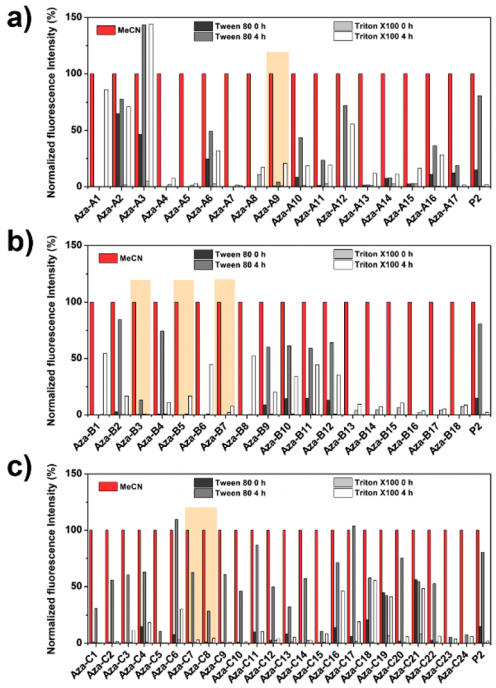

Fig. 4 Normalized fluorescence re-illumination of novel ACQ probes (250 nmol L^{-1} compared with acetonitrile, (a): Type A Aza-BODIPY; (b): Type B Aza-BODIPY; (c): Type C Aza-BODIPY) in surfactant 1% Tween 80 and 1% Triton X100. The excitation was set at the wavelength blue-shifted by 20 nm compared to the maximal absorption wavelength of the probe (slit: 5/5 nm).

brightness of 25 696) possessed preferred NIR absorption and emission. Among the one side rigidified Aza-BODIPYs (Type B) with identical scaffold to **P2**, compounds **Aza-B3**, **Aza-B5**, **Aza-B7**, **Aza-B13–Aza-B18** were found to have preferable re-illumination property. These dyes absorb in the NIR region with absorption maxima longer than 710 nm and emit strongly in the NIR region with fluorescence quantum yields greater than 0.14. Especially notable dyes were **Aza-B3**, **Aza-B5**, and **Aza-B7** with high brightness in the NIR region (Table S4†). As for the dual sides conformationally rigidified Aza-BODIPYs (Type C), we were also fortunate to find that **Aza-C1**, **Aza-C5**, **Aza-C7**, **Aza-C8**, **Aza-C9**, **Aza-C10**, **Aza-C23** and **Aza-C24** could possibly be used to replace **P2**. However, these types of dye often encountered solubility problems, especially for those dyes containing pyridine moiety. Considering the overall balanced properties of absorption maxima, fluorescence brightness and solubility, **Aza-C7** and **Aza-C8** were advantageous (λ_{abs} > 730 nm, brightness >37 000) over **P2** (λ_{abs} > 703 nm, brightness 36 750).

Preparation and characterization of Aza-BODIPY-labeled nanocarriers

From systematic evaluation of BODIPYs and Aza-BODIPYs for ACQ and re-illumination, we identified various structures with the Aza-BODIPY scaffold to be potentially suitable for NDDS studies, and **Aza-C7** and **Aza-C8** were recommended for *in vivo* studies. To demonstrate the advantage of the selected probes, we used **Aza-C7** as an example for further investigations compared with **P2** and **DiR**. In order to evaluate the compatibility of the fluorescent dye with commonly used nanocarriers, probe-encapsulated poly(ethylene glycol)$_{2k}$-poly(D,L-lactic acid)$_{2.5k}$ (mPEG$_{2k}$PDLLA$_{2.5k}$) PMs nanocarriers were prepared and characterized. The particle size, polydispersity index (PDI), zeta potential, and encapsulation efficiency (EE(%)) of the PMs were measured in an aqueous environment (Table S6 and Fig. S4, ESI†). The particle size of the PMs was determined to be about 55 nm and the zeta potential was found to be in the range of ±10 mV.

Under a low concentration of fluorescent dye, the standard curve was tested (Fig. S5, ESI†), and the EE(%) of the nanocarriers was determined. The nanocarriers had high EE(%), which could effectively encapsulate the probe into nanocarriers for study. Stable encapsulation is an important prerequisite for nano-tracer fluorescence imaging. The fluorescence and particle size of the dye-labeled nanocarrier PMs in water were also tested. It could be seen from Fig. S6† that the nanocarriers remained stable for up to 48 h, which further verified the stability of the nanostructure and packaging. This would eliminate the possibility of premature leakage of the physically encapsulated dye, and avoid false signals *in vivo*.

In vivo live imaging and evaluation of re-illumination

To determine the suitability of the preferred dye in NNDSs, biodegradable PMs were selected as nanocarriers. Dye-labeled PMs were studied using the IVIS system, and the fate of the nanocarriers in rats was examined after injection through the tail vein. As shown in Fig. 5, after intravenous administration,

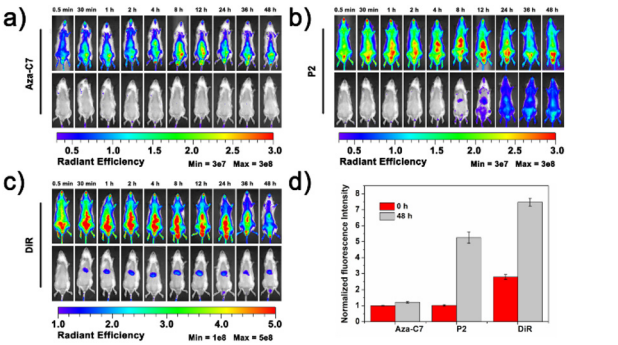

Fig. 5 *In vivo* fluorescence bioimaging of PMs in rats after i.v. administration (0.04285 μmol dye equiv. per kg) under fasted state *via* IVIS live imaging system. (a) **Aza-C7** and (c) **P2**: $\lambda_{ex/em}$ = 710/760 nm; (b) **DiR**: $\lambda_{ex/em}$ = 745/800 nm. (d) Normalized fluorescence intensity of quenched dye in the abdominal area (n = 3).

the fluorescence signals of the **Aza-C7**- and **P2**-labeled PMs rapidly spread throughout the whole rat, and were significantly distributed in the mouth, genitals and hind legs. In the **DiR**-labeled group, the fluorescence signal of the peripheral tissues reached the maximum value at 5 min after administration, and continued to decrease up to 48 h, while the fluorescence intensity of liver fluctuated within 2 h and reached the peak value at 8 h. Although the overall biodistribution pattern of the ACQ probes was similar, the **P2**-and **DiR**-labeled nanocarriers enhanced and amplified the accumulation of PMs in the extremities compared with **Aza-C7**, which had some implications for nanocarrier fate studies. In addition, the **P2**- and **DiR**-quenched groups had obvious fluorescence recurrence, which also interfered with the normal test. As shown in Fig. 5d, **Aza-C7** was found to have decreased fluorescence re-illumination properties over **P2** and **DiR**. A detailed step-by-step description and discussion of *in vivo* live imaging has been published.[49]

Conclusions

ACQ fluorescent dyes have an "ON → OFF" signal conversion mode, which has broad application prospects in the field of NDDSs. Our previous studies have demonstrated the application value of ACQ dye **P2**; however, multiple components in the biological environment may cause the re-illumination of the quenched fluorescent aggregates. To further diminish the potential impact of fluorescent probe-associated artefacts, we studied the quenching properties of different ACQ dyes first. From *in vitro* studies, it was found that Aza-BODIPY dyes have superior ACQ ability. We chose **Aza-C7**-loaded PMs for further investigation. Compared with the analogues of **P2** and **DiR**, **Aza-C7**-loaded PMs have decreased fluorescence re-illumination properties. *In vivo* studies confirmed that **Aza-C7** has advantages over **P2** and commercialized probe **DiR**. Taken together, novel ACQ probes are promising tools for more accurate bioimaging.

Experimental section

Spectrum measurement procedure

A stock solution of the probe (1 mM) was prepared and all absorption (759S UV-visible spectrophotometer) and fluorescence (F98 fluorescence spectrophotometer) measurements were performed in MeCN at room temperature. For the fluorescence measurements, excitation was set at the wavelength blue-shifted by 20 nm compared to the maximal absorption wavelength of the probe (slit: 5/5 nm). The molar extinction coefficient was calculated using the Beer–Lambert law.

The quantum yield was calculated using the following method recommended by Varian (**https://www.jobinyvon.com/usadivisions/Fluorescence/applications/quantumyieldstrad.pdf**, accessed on May 9th, 2022) and was compared with the method reported by Fery-Forgues *et al.*[50]

$$\Phi_u = \Phi_s \cdot \frac{F_u}{F_s} \cdot \frac{A_s}{A_u} \cdot \frac{{\eta_U}^2}{{\eta_S}^2} \quad (1)$$

Φ, F, A and η refer to the fluorescent quantum yield, fluorescent area, absorption and solvent refractive index for the unknown (U) or standard (S), respectively. The fluorescent quantum yield of simple BODIPY is the relative fluorescence quantum yield estimated by using Rhodamine B (Φ = 0.65 in ethanol) as a fluorescence standard. Fluorescent quantum yields of BODIPY were determined *via* eqn (1) in acetonitrile using **P4** (Φ = 0.65, in acetonitrile) as a reference and the fluorescent quantum yields of Aza-BODIPY use **P2** (Φ = 0.35, in acetonitrile) as a reference.

Evaluation of ACQ effect

The ACQ properties were determined by measuring their fluorescence spectra in acetonitrile/water binary systems with different water contents on an F98 fluorescence spectrophotometer. The acetonitrile stock solutions with probe concentrations of 50 μmol L^{-1} were prepared, and 20 μL of stock solution was added into the acetonitrile/water binary systems with different water contents (total 4 mL), so that the final probe concentrations were consistent (250 nmol L^{-1}).

Evaluation of *in vitro* fluorescence re-illumination

To test the fluorescence re-illumination, pre-quenched fluorophore dispersions were prepared by diluting the MeCN stock solutions with ultrapure water by 200-fold. Quenched samples were diluted by 10-fold in 1% Tween-80 solution or 1% Triton X100 (the final probe concentration was 250 nmol mL^{-1}), and incubated at 37 ± 0.5 °C to monitor the changes in their fluorescence intensity over time (0 h and 4 h) *via* an F98 fluorescence spectrophotometer.

Preparation of dye-loaded nanocarriers

Taking **P2** as an example, probe-encapsulated poly(ethylene glycol)$_{2k}$-poly (D,L-lactic acid)$_{2.5k}$ (mPEG$_{2k}$PDLLA$_{2.5k}$) PM nanocarrier was prepared by thin-film dispersion method. 100 mg of mPEG$_{2k}$PDLLA$_{2.5k}$ and 100 μg of **P2** were dissolved in 10 mL of dichloromethane and evaporated at 60 °C to form a homogeneous film. The film was hydrated in 20 mL of deionized water at 60 °C under mild stirring (500 rpm) for 1 h. The dispersion was filtered through a 0.22 μm filter to obtain the PM solution. All formulations were stored at 4 °C for future use.

Characterization of fluorescently labeled nanocarriers

The particle size and zeta potential of all fluorescent formulations were measured at ambient temperature (Malvern Zetasizer Nano ZSP). All measurements were performed after diluting the formulations to an appropriate concentration with deionized water. The EE% was measured by an ultrafiltration method. The details of this method were provided in the previous work.[37]

In vivo imaging

Male SD rats weighing 180 ± 20 g were selected. All animal procedures were performed in accordance with the Guidelines for Care and Use of Laboratory Animals of Fudan University and approved by the Animal Ethics Committee of Fudan University. Before the experiment, to reduce the autofluorescence from the hair, the abdominal hair of the rats should be removed. After that, all animals were fasted but allowed free access to water for 12 h. Fluorescent dye-labeled PMs and their pre-quenched dispersions were injected through the tail vein. The injection volume was calculated as 0.04285 μmol per kg of rat, and three rats were selected for each group. An IVIS real-time imaging system was used to detect the fluorescence signals at 5 min, 0.5 h, 1 h, 2 h, 4 h, 8 h, 12 h, 24 h, 36 h, and 48 h after drug administration. The excitation/emission wavelength of Aza-BODIPY probes (**P2** and **Aza-C7**) was set at 710/760 nm, and that of DiR was set at 745/800 nm.

Author contributions

Xin Ji: Conceptualization, methodology, investigation, validation, writing – original draft. Yifan Cai: Investigation, writing – original draft. Xiaochun Dong: Conceptualization, supervision, writing – review & editing. Wei Wu: Conceptualization, methodology, writing – review & editing. Weili Zhao: Conceptualization, methodology, writing – review and editing.

Conflicts of interest

There are no conflicts to declare.

Acknowledgements

We thank Shanghai Energy Biopharma Co., Ltd (ALA@energy) for kindly providing the fluorescent dyes. We thank the National Natural Science Foundation of China (No. 82030107) for financial support of this project.

References

1 A. Singh and M. M. Amiji, *Curr. Opin. Biotechnol.*, 2022, **74**, 241–246.
2 J. Shi, A. R. Votruba, O. C. Farokhzad and R. Langer, *Nano Lett.*, 2010, **10**, 3223–3230.
3 D. A. LaVan, D. M. Lynn and R. Langer, *Nat. Rev. Drug Discovery*, 2002, **1**, 77–84.
4 S. Talebian, J. Foroughi, S. J. Wade, K. L. Vine, A. Dolatshahi-Pirouz, M. Mehrali, J. Conde and G. G. Wallace, *Adv. Mater.*, 2018, **30**, e1706665.
5 H. Cabral, K. Miyata, K. Osada and K. Kataoka, *Chem. Rev.*, 2018, **118**, 6844–6892.
6 Y. Wang, Y. Zhang, J. Wang and X. J. Liang, *Adv. Drug Delivery Rev.*, 2019, **143**, 161–176.
7 Y. Malam, M. Loizidou and A. M. Seifalian, *Trends Pharmacol. Sci.*, 2009, **30**, 592–599.
8 G. Griffiths, B. Nyström, S. B. Sable and G. K. Khuller, *Nat. Rev. Microbiol.*, 2010, **8**, 829–834.
9 D. Chen, S. Lian, J. Sun, Z. Liu, F. Zhao, Y. Jiang, M. Gao, K. Sun, W. Liu and F. Fu, *Drug Delivery*, 2016, **23**, 808–813.
10 V. P. Torchilin, *Nat. Rev. Drug Discovery*, 2014, **13**, 813–827.
11 Y. Barenholz, *J. Controlled Release*, 2012, **160**, 117–134.
12 V. P. Torchilin, *Nat. Rev. Drug Discovery*, 2014, **13**, 1–15.
13 M. A. Eaton, L. Levy and O. M. Fontaine, *Nanomedicine*, 2015, **11**, 983–992.
14 J. K. Patra, G. Das, L. F. Fraceto, E. V. R. Campos, M. D. P. Rodriguez-Torres, L. S. Acosta-Torres, L. A. Diaz-Torres, R. Grillo, M. K. Swamy, S. Sharma, S. Habtemariam and H. S. Shin, *J. Nanobiotechnol.*, 2018, **16**, 71.
15 D. L. Stirland, J. W. Nichols, S. Miura and Y. H. Bae, *J. Controlled Release*, 2013, **172**, 1045–1064.
16 R. J. Hicks and M. S. Hofman, *Nat. Rev. Clin. Oncol.*, 2012, **9**, 712–720.
17 S. S. Gambhir, *Nat. Rev. Cancer*, 2002, **2**, 683–693.
18 D. J. Brenner and E. J. Hall, *N. Engl. J. Med.*, 2007, **357**, 2277–2284.
19 R. Huzjan, E. Sala and H. Hricak, *Nat. Clin. Pract. Urol.*, 2005, **2**, 434–442.
20 J. Qi, X. Hu, X. Dong, Y. Lu, H. Lu, W. Zhao and W. Wu, *Adv. Drug Delivery Rev.*, 2019, **143**, 206–225.
21 P. J. Photos, L. Bacakova, B. Discher, F. S. Bates and D. E. Discher, *J. Controlled Release*, 2003, **90**, 323–334.
22 Y. Sheng, Y. Yuan, C. Liu, X. Tao, X. Shan and F. Xu, *J. Mater. Sci.: Mater. Med.*, 2009, **20**, 1881–1891.
23 L. Basile, C. Passirani, N. T. Huynh, J. Bejaud, J. P. Benoit, G. Puglisi and R. Pignatello, *Int. J. Pharm.*, 2012, **426**, 231–238.
24 Y. Zhang, C. Wang, C. Xu, C. Yang, Z. Zhang, H. Yan and K. Liu, *Chem. Commun.*, 2013, **49**, 7286–7288.
25 H. He, C. Liu, Y. Lv, J. Qi, Y. Lu, X. Dong, W. Zhao and W. Wu, *Aggregate*, 2022, **3**, e163.
26 G. Lu, X. Gao, H. Zhang, Y. Zhang, Y. Yu, Z. Sun, W. Li, W. Wu, Y. Lu and H. Zou, *Chin. Chem. Lett.*, 2022, **33**, 1923–1926.
27 D. M. Charron and G. Zheng, *Nano Today*, 2018, **18**, 124–136.
28 D. Zhai, W. Xu, L. Zhang and Y. T. Chang, *Chem. Soc. Rev.*, 2014, **43**, 2402–2411.
29 N. Calander, *Anal. Chem.*, 2004, **76**, 2168–2173.
30 X. Ma, R. Sun, J. Cheng, J. Liu, F. Gou, H. Xiang and X. Zhou, *J. Chem. Educ.*, 2015, **93**, 345–350.
31 A. C. Grimsdale, K. L. Chan, R. E. Martin, P. G. Jokisz and A. B. Holmes, *Chem. Rev.*, 2009, **109**, 897–1091.
32 V. M. Weiss, H. Lucas, T. Mueller, P. Chytil, T. Etrych, T. Naolou, J. Kressler and K. Mader, *Macromol. Biosci.*, 2018, **18**, 1700240.
33 Q. Shuai, G. Zhao, X. Zhang, B. Yu, R. J. Lee and W. K. Su, *Colloids Surf., B*, 2019, **181**, 872–878.
34 F. Meng, J. Wang, Q. Ping and Y. Yeo, *ACS Nano*, 2018, **12**, 6458–6468.
35 W. Q. Li, J. Y. Wu, D. X. Xiang, S. L. Luo, X. B. Hu, T. T. Tang, T. L. Sun and X. Y. Liu, *Int. J. Nanomed.*, 2019, **14**, 8345–8360.
36 R. Ngoune, A. Peters, D. von Elverfeldt, K. Winkler and G. Pütz, *J. Controlled Release*, 2016, **238**, 58–70.
37 X. Hu, J. Zhang, Z. Yu, Y. Xie, H. He, J. Qi, X. Dong, Y. Lu, W. Zhao and W. Wu, *Nanomedicine*, 2015, **11**, 1939–1948.
38 X. Hu, W. Fan, Z. Yu, Y. Lu, J. Qi, J. Zhang, X. Dong, W. Zhao and W. Wu, *Nanoscale*, 2016, **8**, 7024–7035.
39 E. Ahmad, Y. Feng, J. Qi, W. Fan, Y. Ma, H. He, F. Xia, X. Dong, W. Zhao, Y. Lu and W. Wu, *Nanoscale*, 2017, **9**, 1174–1183.
40 F. Xia, W. Fan, S. Jiang, Y. Ma, Y. Lu, J. Qi, E. Ahmad, X. Dong, W. Zhao and W. Wu, *ACS Appl. Mater. Interfaces*, 2017, **9**, 21660–21672.
41 C. Shen, Y. Yang, B. Shen, Y. Xie, J. Qi, X. Dong, W. Zhao, W. Zhu, W. Wu, H. Yuan and Y. Lu, *Nanoscale*, 2017, **10**, 436–450.
42 Y. Yang, Y. Lv, C. Shen, T. Shi, H. He, J. Qi, X. Dong, W. Zhao, Y. Lu and W. Wu, *Acta Pharm. Sin. B*, 2021, **11**, 1056–1068.
43 D. Liu, B. Wan, J. Qi, X. Dong, W. Zhao, W. Wu, Y. Dai, Y. Lu and Z. Chen, *Chin. Chem. Lett.*, 2018, **29**, 1834–1838.
44 W. Fan, H. Peng, Z. Yu, L. Wang, H. He, Y. Ma, J. Qi, Y. Lu and W. Wu, *Acta Pharm. Sin. B*, 2022, **12**, 2479–2493.
45 I. Zoya, H. He, L. Wang, J. Qi, Y. Lu and W. Wu, *Chin. Chem. Lett.*, 2021, **32**, 1545–1549.
46 Y. Yang, Y. Lv, C. Shen, T. Shi, H. He, J. Qi, X. Dong, W. Zhao, Y. Lu and W. Wu, *Acta Pharm. Sin. B*, 2021, **11**, 1056–1068.
47 Y. Li, C. Wang, S. Zong, J. Qi, X. Dong, W. Zhao, W. Wu, Q. Fu, Y. Lu and Z. Chen, *J. Biomed. Nanotechnol.*, 2019, **15**, 686–702.
48 E. Ahmad, Y. Lv, Q. Zhu, J. Qi, X. Dong, W. Zhao, Z. Chen, W. Wu and Y. Lu, *Appl. Mater. Today*, 2020, **19**, 100556.
49 Y. Cai, X. Ji, Y. Zhang, C. Liu, Z. Zhang, Y. Lv, X. Dong, H. He, J. Qi, Y. Lu, D. Ouyang, W. Zhao and W. Wu, *Aggregate*, 2022, e277.
50 S. Fery-Forgues and D. Lavabre, *J. Chem. Educ.*, 1999, **76**, 1260.

